Insight into the SO2 poisoning mechanism for NOx removal by NH3-SCR over Cu/LTA and Cu/SSZ-13

Chemical Engineering Journal 395 (2020) 125048

Contents lists available at ScienceDirect

Chemical Engineering Journal

journal homepage: www.elsevier.com/locate/cej

Insight into the SO_2 poisoning mechanism for NO_x removal by NH_3-SCR over Cu/LTA and Cu/SSZ-13

Aiyong Wang, Louise Olsson*

Competence Centre for Catalysis, Chemical Engineering, Chalmers University of Technology, Gothenburg, SE 412 96, Sweden

HIGHLIGHTS

- Cu/LTA and Cu/SSZ-13 were synthesized and examined for SO_2 poisoning.
- $[Cu(OH)]^+$ in Cu/LTA is found to be more vulnerable to SO_2 than Cu/SSZ-13.
- In SCR condition with SO_2, Cu/LTA can store more SO_2 than Cu/SSZ-13.
- Cu/LTA exhibit a slower deactivation rate than Cu/SSZ-13.
- 750 °C fully regenerates Cu/LTA, while Cu/SSZ-13 show some loss at high temperature.

GRAPHICAL ABSTRACT

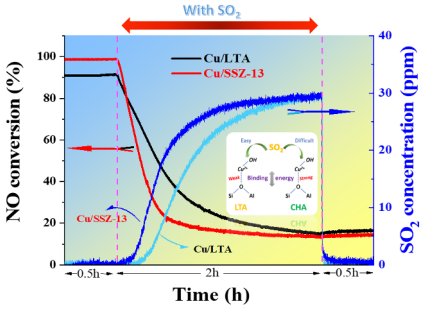

ARTICLE INFO

Keywords:
Cu
LTA
SSZ-13
Standard SCR
Fast SCR
SO_2

ABSTRACT

In this study, Cu/LTA and Cu/SSZ-13 catalysts are examined for sulfur poisoning and regeneration. The nature of the Cu species was probed with H_2-TPR and *in-situ* DRIFTS. These characterizations collectively indicate that primarily Z2Cu is present in Cu/LTA, whereas Cu/SSZ-13 contains a higher concentration of ZCuOH. ZCuOH is proved to be more vulnerable to SO_2 poisoning than Z2Cu sites in both Cu/zeolites. H_2-TPR results suggest that the interaction of ZCuOH with the framework in Cu/LTA is much weaker than in Cu/SSZ-13, thereby leading to more susceptibility to SO_2 adsorption. Moreover, Cu/LTA can store more SO_2 under NH_3-SCR conditions in the presence of SO_2, and it also has a slower deactivation rate due to the different location of generated $(NH_4)_2SO_4$. Cu/LTA can be fully restored after regeneration at 750 °C. However, Cu/SSZ-13 experiences a loss of activity at high temperature, which is attributed to newly formed CuO_x clusters.

1. Introduction

The selective catalytic reduction (SCR) method developed in the 1970s has high efficiency and is currently the most widely used process for industrial NO_x removal [1]. In this method, the reducing agents used are CO or H_2 [2–4], various hydrocarbons [5–7], and NH_3 [8–12]. The catalysts are (un)supported non-noble metal oxides (V_2O_5-WO_3/TiO_2, MnO_x, etc.) [13–17], supported noble metals (Ag/Al_2O_3, etc.) [18–20], and zeolite catalysts (Cu or Fe/BEA, CHA, FER, etc.) [21–25]. Moreover, ammonia selective catalytic reduction (NH_3-SCR, $4NH_3 + 4NO + O_2 \rightarrow 4\ N_2 + 6H_2O$) has become the primary technology for the abatement of NO_x emissions from diesel engines [26,27]. The ammonia is produced through the thermal decomposition and hydrolysis of aqueous urea ($CO(NH_2)_2 + H_2O \rightarrow 2NH_3 + CO_2$). Copper-exchanged chabazite (CHA) framework zeolites, e.g., Cu/SSZ-13, have been extensively studied and practically applied in the last decade as NH_3-SCR catalysts for NO_x abatement in diesel vehicles [8,28–32]. However, with long-term exposure to harsh temperatures,

* Corresponding author.
E-mail address: louise.olsson@chalmers.se (L. Olsson).

https://doi.org/10.1016/j.cej.2020.125048
Received 16 January 2020; Received in revised form 8 April 2020; Accepted 9 April 2020
Available online 11 April 2020

e.g., 800 °C, which occasionally occurs for regeneration purposes, a Cu/SSZ-13 catalyst has a high risk of degradation, which leads to catalyst deactivation [33]. Hong's group [34] has recently found that high-framework silica Cu/LTA zeolite is a more robust SCR catalyst that withstands hydrothermal aging even at 900 °C and maintains remarkable NH_3-SCR activity. We have confirmed this extraordinary stability and investigated the mechanism for the unusual stability of Cu/LTA catalyst [35].

Cu/zeolites adapted in the Exhaust Aftertreatment System (EATS), whether CHA or LTA framework topology, inevitably undergo sulfur (e.g., SO_2) contamination because of the presence of ppm levels of sulfur (< 15 ppm) in commercial fuel, even under the Ultra-Low Sulfur Diesel (ULSD) regulation [36–39]. In-depth studies of Cu-chabazite SCR catalysts, including Cu/SSZ-13 and Cu/SAPO-34, have reported on the effect of sulfur poisoning [36,39–44]. In general, two main deactivation processes are suggested: chemical and physical. Kumar et al. [41] have investigated various effects of SO_2 and SO_3 on Cu/CHA SCR catalysts and found that the presence of SO_3 resulted in a large impact on catalytic performance. Similar results have also been reported by Cheng and coworkers [40], who propose that the formation of $CuSO_4$ upon SO_3 poisoning can be responsible for the deactivation. Several studies [38,42] are available regarding the impact of SO_2 on Cu/CHA catalysts (SAPO-34 or SSZ-13), and it is suggested that the formation of ammonium sulfate species may poison the active sites and also block zeolite pores. Li's group [45] have compared sulfate formation on Cu/SSZ-13 and Cu/SAPO-34 catalysts, and have found three sulfate species on the catalyst surface, i.e., H_2SO_4, $CuSO_4$, and $Al_2(SO_4)_3$. Wijayanti et al. [46] have also found that H_2O and hydrothermal aging can significantly promote the formation of copper sulfates.

Pioneering work by Kwak et al. [47] has shown that Cu ions primarily occupy sites in the 6-membered rings at low ion exchange levels, while these ions are mostly present in the large cages of the CHA structure at high ion exchange levels. On this basis, later research [32,48] further identified that these two distinct Cu cationic species are: (1) ion-exchanged Cu^{2+} ions with two neighboring framework Al in 6-membered rings that provide two negative framework charges (Z2Cu); and (2) $[Cu(OH)]^+$ with one framework Al in the 8-membered rings needed one negative framework charge (ZCuOH). Subsequently, the effect of sulfur on Z2Cu and ZCuOH sites was studied in-depth [36,49], and the results show that the extent to which these two Cu species are poisoned by sulfur are extremely different. ZCuOH more readily interacts with SO_2 than Z2Cu does, and this interaction leads to the formation of highly stable sulfur species. This hypothesis is further supported by theoretical first-principle simulations [39].

Overall, previous studies have systematically explored the effects of sulfur poisoning on state-of-the-art Cu/CHA catalysts (i.e., Cu/SSZ-13 and Cu/SAPO-34) and have demonstrated the sulfur sensitivity of these small-pore molecular sieves. Nonetheless, little attention has been paid to the impact of sulfur on Cu/LTA catalysts mainly because Cu/LTA as a SCR catalyst is currently fairly novel. To the best of our knowledge, only the study by Ryu et al. [34] mentions SO_2 poisoning of Cu/LTA catalysts, and that study only conducted one simple SO_2 (20 ppm) exposure effect on NH_3-SCR activity without any further characterization studies. Thus, the influence of sulfur poisoning on the active sites and the poisoning mechanisms of Cu/LTA, which is a potential next generation SCR catalyst, have still not been studied.

The present study compares the newly emerged Cu/LTA catalyst with the state-of-the-art Cu/SSZ-13 catalyst. Two model samples with analogous chemical components, i.e., Cu/LTA and Cu/SSZ-13 (Si/Al ~ 15, Cu/Al ~ 0.45), were prepared for sulfur poisoning and regeneration investigations. The fresh and sulfated materials were further characterized with a number of spectroscopic methods, including H_2-TPR, *in-situ* DRIFTS, various SO_2-TPD and NH_3-TPD, in order to elucidate the catalyst structure/function relationships and to attain insight into the catalytic deactivation mechanism upon sulfur poisoning.

2. Experimental section

2.1. Catalyst synthesis

Both Na/SSZ-13 (Si/Al ~ 15) and H/LTA (Si/Al ~ 15) were hydrothermally synthesized in-house using methods previously reported [35,50,51]. After synthesis, separation, drying, and calcination, the obtained Na/SSZ-13 was ion-exchanged with a 5.4 M NH_4NO_3 solution twice for 1 h at 80 °C to obtain NH_4/SSZ-13. Then the NH_4/SSZ-13 was calcined again to obtain H/SSZ-13. Cu/zeolites (i.e., SSZ-13 and LTA) were prepared using the incipient wetness impregnation (IWI) method. The details can be found in our prior publication [35]. Briefly, a certain amount of $Cu(NO_3)_2{\cdot}2.5H_2O$ was added to ethanol while stirring until completely dissolved. Then the zeolite (H/LTA or H/SSZ-13) was slowly introduced into the solution, and the mixture vessel was capped and stirred for 15 min. After this, the product was dried at room temperature overnight in a fume hood.

The as-prepared powder was fully ground before calcination at 600 °C for 8 h, then ramped up to 750 °C for 2 h in static air. The obtained powder was used to coat a monolith (400 cpsi) that was 15 mm in diameter and 20 mm in length. The details of the washcoat procedure can be found in our prior work [52]. Alumina (Disperal P2, Sasol) was used as a binder when coating the zeolite to increase the attachment of the zeolite, with a ratio of around 95/5 between the zeolite and binder. The total washcoat weight was ~300 mg, including the binder. The prepared monolith was then calcined at 500 °C for 2 h. Prior to use, the monolith was first degreened at 750 °C for 4 h under standard SCR reaction conditions (400 ppm NO, 400 ppm NH_3, 5% H_2O, 10% O_2, 1200 ml/min) in a flow reactor (described in Section 2.3). This step can further facilitate the movement of copper species into ion-exchanged positions, and indeed we observed that the color of the samples changed from grayish blue to pure blue.

2.2. Catalyst characterization

The Cu, Si, and Al contents of the samples were measured with Inductively Coupled Plasma Atomic Emission Spectroscopy (ICP-AES) conducted by ALS Scandinavia AB.

H_2 temperature-programmed reduction (H_2-TPR) of the samples was performed on a Differential Scanning Calorimeter (Sensys DSC, Setaram) connected to a mass spectrometer (Hiden HPR-20 QUI MS) to detect outlet gases. Measurements were conducted on both fresh and sulfated samples (i.e., Cu/LTA and Cu/SSZ-13). Sulfated samples were first exposed to SO_2 (400 ppm NO, 400 ppm NH_3, 30 ppm SO_2, 10% O_2, 5% H_2O, and balance Ar) at 250 °C for 2 h in a flow reactor (see Section 2.3). TPR was conducted from room temperature to 800 °C at 10 °C/min in 2000 ppm H_2 balanced with Ar. Note that no pretreatment was performed on the samples prior to the TPR experiments.

In-situ Diffuse Reflectance Infrared Fourier Transform Spectra (DRIFTS) were acquired with a Bruker Vertex 70 spectrometer, equipped with an MCT detector and operated at 4 cm^{-1} resolution. Each spectrum reported was obtained by averaging 256 scans. Prior to each measurement, the catalysts were pretreated by heating in 100 ml/min 10% O_2/Ar to 500 °C and maintained at this temperature for 1 h. The ZCuOH and Z2Cu species were studied through framework internal asymmetric T-O-T vibrations [53]. This was done by cooling the catalysts to 200 °C to carry out the adsorption of NH_3 (300 ppm NH_3, 10% O_2, balance Ar) until saturation. Subsequently, the catalyst was purged in 10% O_2/Ar for 20 min, which was followed by NO exposure (300 ppm NO, 10% O_2, balance Ar) for 3 h. The spectra were recorded as a function of time using the background measured at 200 °C in a flow of 10% O_2/Ar, prior to the introduction of NH_3. To study SO_2 poisoning, the catalysts were first exposed to SO_2 (30 ppm SO_2, 10% O_2, balance Ar) at 200 °C for 2 h and spectra were taken.

NH_3 temperature-programmed desorption (NH_3-TPD) was carried out using a flow reactor system with NH_3 detection via an online MKS

2030 FTIR analyzer (see Section 2.3). The same monoliths (~300 mg catalyst) used for the SCR reactions (see Section 2.3) were used for the NH_3-TPD measurements, and the experimental steps were as follows: (1) heat the sample to 500 °C in 10% O_2/Ar (1200 ml/min) and keep at 500 °C for 20 min; (2) cool the sample to NH_3 adsorption temperatures of 100 °C in 10% O_2/Ar; (3) adsorb NH_3 (400 ppm NH_3, 10% O_2, 5% H_2O, 30 ppm SO_2 (if needed)) in Ar until the outlet NH_3 concentrations remained constant for 1 h; (4) flush the catalyst with 10% O_2 in Ar, and 5% H_2O , 30 ppm SO_2 (if needed); (5) then purge with Ar for 20 min at the adsorption temperature (i.e., 100 °C); and (6) ramp from the adsorption temperature to 750 °C at 20 °C/min, and maintaining the temperature at 750 °C for 20 min.

SO_2 temperature-programmed desorption (SO_2-TPD) was performed using the same procedure as described above for NH_3-TPD. A new monolith was used for each sulfur TPD experiment with the same batch of Cu/LTA and Cu/SSZ-13. Briefly, the experimental steps were as follows: (1) heat the monolith sample to 500 °C in 10% O_2/Ar (1200 ml/min) and keep at 500 °C for 20 min; (2) cool the sample to the SO_2 adsorption temperature of 250 °C in 10% O_2/Ar; (3) adsorb SO_2 (30 ppm SO_2, 10% O_2 in Ar, 5% H_2O (if needed), 400 ppm NH_3 (if needed)) until outlet SO_2 concentrations remained constant for 2 h; (4) turn off the SO_2 flow, and flush with 5% H_2O (if needed), 400 ppm NH_3 (if needed) and 10% O_2; (5) then purge with Ar for 20 min at the adsorption temperature (i.e., 250 °C); and (6) ramp from the adsorption temperature to 750 °C using a ramp speed of 20 °C/min, and maintain the temperature at 750 °C for 20 min.

2.3. Reaction tests

NH_3-SCR reactions were conducted on washcoated monoliths in a flow reactor. Details about the reactor system can be found in our previous publication [52]. Briefly, the gases were mixed using several Bronkhorst MFCs, and the water was added with a Bronkhorst CEM system. Concentrations of reactants and products were measured with an online MKS 2030 FTIR analyzer. For a standard SCR reaction ($4NO + 4NH_3 + O_2 \rightarrow 4\,N_2 + 6H_2O$), the feed gas contained 400 ppm NO, 400 ppm NH_3, 10% O_2, 5% H_2O with Ar as the inert balance. For a fast SCR reaction ($NO + NO_2 + 2NH_3 \rightarrow 2\,N_2 + 3H_2O$), 400 ppm NO was replaced with 200 ppm NO and 200 ppm NO_2. The other feed was the same as for a standard SCR reaction. Measurements were conducted from high to low reaction temperatures, and monoliths were maintained at each target temperature for 30 min. Note that steady state was not attained at 150 °C, and the last point was shown for the conversion. All the gas lines were maintained above 100 °C to avoid water condensation. The total gas flow was 1200 sccm, and the gas hourly space velocity (GHSV) was estimated to be 22100 h^{-1} for the monolith (with a washcoat amount of ~300 mg).

Both standard SCR and fast SCR reactions were conducted on fresh, sulfated, and different temperature-regenerated (i.e., 400, 500, 600, and 750 °C) samples. First, the catalyst was degreened using 5% H_2O, 10% O_2 in Ar at 750 °C for 4 h. Thereafter, the activity was measured for standard SCR and fast SCR reactions. For the fresh catalyst a pre-treatment was done prior to each experiment (500 °C for 20 min using 5% H_2O, 10% O_2 in Ar). Note that no pre-treatment was done after poisoning. Thereafter, the temperature was set to 250 °C and maintained at this temperature for 0.5 h under standard SCR conditions (400 ppm NO, 400 ppm NH_3, 10% O_2, 5% H_2O and balance Ar). This was followed by adding 30 ppm SO_2 to the feed gas for 2 h, followed by a purge in the SCR gas phase again for 0.5 h (SO_2 was turned off). After this, the sulfate samples were continuously regenerated at 400, 500, 600, and 750 °C with standard and fast SCR tests between each regeneration temperature.

3. Results and discussion

In this work, we compared two types of Cu/zeolites, Cu/LTA and Cu/SSZ-13, with analogous chemical compositions. As shown in Table 1, the Si/Al ratios of Cu/LTA and Cu/SSZ-13 were 14.4 and 15.2, respectively, and the corresponding Cu/Al ratios were 0.47 and 0.44. Note that, in this study, an Si/Al ratio close to 15 of the zeolites was selected since this ratio is close to the commercial catalysts applied in the EATS of diesel vehicles [53,54]. A Cu/Al ratio close to but less than 0.5 was preferred for Cu loading (e.g., 0.47 for Cu/LTA). This not only avoids the formation of abundant CuO_x clusters but also achieves the utmost catalytic activity [34,48].

Table 1
ICP-AES results for the Cu/LTA and Cu/SSZ-13 samples.

sample	Si content (wt.%)	Al content (wt.%)	Cu content (wt.%)	Si/Al ratio	Cu/Al ratio
Cu/LTA	38.9	2.6	2.9	14.4	0.47
Cu/SSZ-13	37.8	2.4	2.5	15.2	0.44

3.1. H_2-TPR results

H_2-TPR was conducted from ambient conditions without any pre-treatment to investigate the reducibility of fresh and sulfated Cu/zeolites. Fig. 1 shows the H_2-TPR results for the Cu/LTA and Cu/SSZ-13 samples. First, two distinct reduction peaks were observed in the fresh catalysts from the TPR curves for both Cu/LTA and Cu/SSZ-13, which was expected. It has previously been suggested that the ZCuOH can be anticipated to show a reduction peak at a lower temperature since the binding energy with the framework of ZCuOH is lower than that of Z2Cu [35]. Therefore, the low-temperature reduction peaks at 213 and 376 °C for fresh Cu/LTA and Cu/SSZ-13, respectively, were attributed to $[Cu(OH)]^+$ (i.e., ZCuOH) → Cu^+. And the corresponding high-temperature peaks, occurring at 488 and 457 °C, were attributed to the reduction of Cu^{2+} (i.e., Z2Cu) to Cu^+. Since the reduction of Cu^+ to Cu^0 requires the degradation of the zeolite framework, the reaction process typically occurs above 800 °C [55,56]. This exceeded the measurement range of our instrument (25–800 °C), thus, we could not detect the reduction feature in terms of $Cu^+ \rightarrow Cu^0$. One key feature that we found, however, was a dramatic reduction temperature discrepancy regarding ZCuOH between fresh Cu/LTA and Cu/SSZ-13 samples, i.e., 213 versus 376 °C, which is approximately a 160 °C difference. Meanwhile, Z2Cu was reduced by H_2 at comparable temperatures (488 and 457 °C). According to the literature, the H_2-TPR reduction peaks of ZCuOH and Z2Cu were different in the same type of Cu/zeolite. There are many possible reasons for this, such as Si/Al ratios, Cu loadings, and the TPR conducted conditions (e.g., ramp rate).

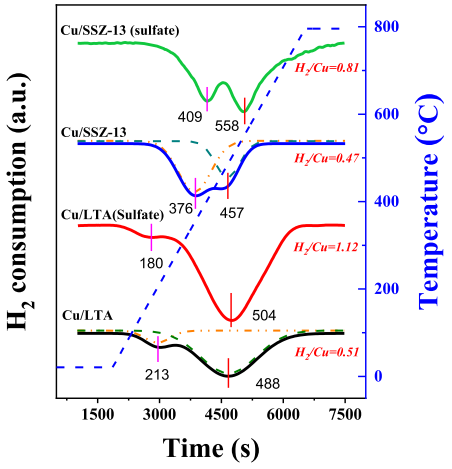

Fig. 1. H_2-TPR curves for the fresh and sulfated Cu/LTA and Cu/SSZ-13 samples.

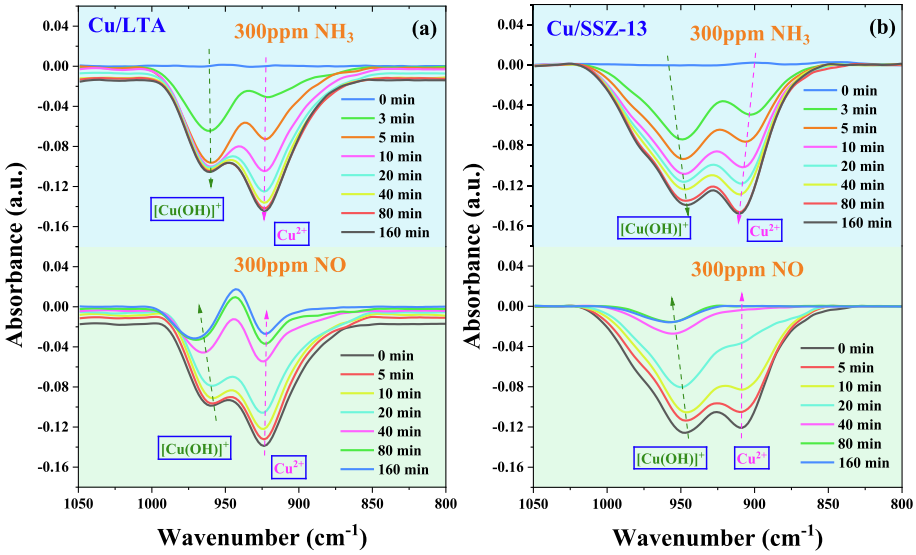

Fig. 2. DRIFTS spectra of T-O-T vibrational region perturbed by NH_3 adsorption (upper panels) and followed by NO feeding to react with preadsorbed NH_3 over time (lower panels) for (a) Cu/LTA and (b) Cu/SSZ-13.

However, in this work, we controlled these conditions using similar Si/Al ratios, similar Cu loadings, and the TPR conditions for Cu/LTA and Cu/SSZ-13 samples were identical. Since we observe such a large gap (213 vs 376 °C) for reduction of ZCuOH, we suggest that this should be mainly due to the different ZCuOH binding energy in Cu/LTA compared to Cu/SSZ-13. Therefore, it can be inferred that, in comparison to Cu/SSZ-13, ZCuOH residing in Cu/LTA is likely to have a much lower binding energy to the framework, resulting in an lower reduction temperature.

To obtain the distribution in Z2Cu and ZCuOH of Cu/LTA and Cu/SSZ-13 samples, peak fitting was used to determine the ratios based on the area of these two Cu species for fresh samples. Briefly, in Cu/LTA, the TPR showed 12% of the ZCuOH sites and 88% of the Z2Cu sites. Meanwhile, ZCuOH was shown to be the dominant Cu site in the Cu/SSZ-13 sample, where 65% of the populations were from TPR. This is an interesting finding. Previous studies have shown that Cu/LTA is more resistant to high-temperature hydrothermal aging than Cu/SSZ-13 is [34,35,57]. The conversion of ZCuOH to CuO_x is widely believed to be the main cause of high-temperature deactivation in Cu/SSZ-13. We have earlier found an unusual stability of ZCuOH under different harsh aging temperatures up to 900 °C, which might be one of the reasons for the extraordinary hydrothermal stability of the Cu/LTA sample, together with the stability of Brønsted acid sites and the conversion of CuO_x to active Cu sites upon aging [35]. In addition, there was also a significantly larger amount of Z2Cu in the Cu/LTA sample, and this could be another reason for the extraordinary stability of Cu/LTA. Another key feature that we propose based on the different concentrations of Cu species, i.e., Z2Cu and ZCuOH, is the difference in Al distribution among these two zeolites. Specifically, it is clear that Z2Cu needs two Al nearby for charge balance, whereas only one Al is needed for ZCuOH. Therefore, the significantly higher content of Z2Cu in the Cu/LTA sample suggests that more of the Al sites in the LTA are located in pairs in the zeolite framework, as is required for Z2Cu formation. However, this was not case for the Cu/SSZ-13 sample.

The sulfated Cu/LTA and Cu/SSZ-13 samples showed significantly higher H_2 consumption than the fresh samples, as displayed in Fig. 1. A similar phenomenon has also been found by Wijayanti et al. and Shen et al. [38,43] who studied the SO_2 poisoning of Cu/SSZ-13 and Cu/SAPO-34 catalysts, respectively. The total H_2 consumption, i.e., the H_2/Cu ratio, over fresh and sulfated samples was calculated by integrating the peaks from 25 to 800 °C (2000 ppm H_2 as a feed). The H_2/Cu ratios for the fresh samples were determined to be 0.51 and 0.47 for Cu/LTA and Cu/SSZ-13, respectively, which is in line with our discussion above that divalent Cu ions, including ZCuOH and Z2Cu, only undergo a reduction of one-electron below 800 °C [36,48,58]. Note that even though the ratio of H_2/Cu in Cu/zeolites is ca 0.5, we cannot rule out the existence of small amounts of CuO_x.

The total H_2 consumption per Cu for the two sulfated Cu/zeolites were different; 1.12 and 0.81 for sulfated Cu/LTA and Cu/SSZ-13 samples, respectively. Thus, in terms of the H_2 consumption, it can clearly be seen that the Cu/LTA sample was more influenced by SO_2 poisoning. According to Shen et al and He et al [43,59], the higher H_2 consumption of the sulfated Cu/zeolites can be attributed to: (1) the reduction of the sulfated Cu species from the divalent to the metallic state, which only requires one single step ($Cu^{2+} \rightarrow Cu^0$); and (2) the reaction of H_2 with sulfate species. Point (2) has been confirmed in earlier studies (MS) [38,43] in which H_2S formation was observed at around 650 °C for SO_2 poisoned samples using mass spectrometry. This finding was also indirectly demonstrated in the present study by the fact that the H_2/Cu ratio of sulfated Cu/LTA (~1.12) exceeded one, since one copper ion requires, at the most, one H_2 molecule.

3.2. *In situ* DRIFTS results

Based on the perturbation to asymmetric T-O-T vibrations of the zeolite framework, Z2Cu ions residing close to pair Al sites and ZCuOH ions close to single Al sites can clearly be distinguished in Cu/zeolites (e.g., SSZ-13 or LTA), especially with the help of NH_3 [31,33,49]. Therefore, to further investigate the effect of these two types of zeolite structure on the distribution of Cu species and the impact on SCR reactions, in situ DRIFTS of NH_3 adsorption followed by NO feeding over time were conducted. The results are shown in Fig. 2**a** and **b**, for Cu/LTA and Cu/SSZ-13, respectively. Prior to measurements, the samples were dehydrated in 10% O_2/Ar for 1 h at 500 °C to exclude perturbation from H_2O. Backgrounds were measured at 200 °C in a flow of 10% O_2/Ar.

Two well-resolved negative bands were clearly observed for both Cu/LTA and Cu/SSZ-13 samples. Compared with Cu/SSZ-13, Cu/LTA exhibited a shift in the IR signals to higher wavenumbers, which has been observed previously [35,60]. Specifically, as we can see from Fig. 2**a** and **b**, features at approximately 925 and 960 cm^{-1} were detected for Cu/LTA, while slightly lower signals at 900 and 950 cm^{-1} were detected for Cu/SSZ-13. These features corresponded to Z2Cu and ZCuOH species, respectively [53,60]. The signal shift is suggested to be

due to the difference in framework structure between LTA and CHA topology. As shown in the upper panels of Fig. 2**a** and **b**, the samples were fully saturated within 160 min during the NH_3 adsorption step. The evolution of these two Cu species over time upon NH_3 adsorption gives interesting information regarding these two Cu/zeolites. For example, NH_3 preferentially adsorbed onto the ZCuOH sites of the Cu/LTA sample, i.e., 960 cm^{-1} (Fig. 2**a**), where the signal intensity of ZCuOH sites increased significantly faster than the intensity of the signal of the Z2Cu sites. The ZCuOH sites were saturated after only approximately 5 min. This was perhaps due to the stronger interaction between the ZCuOH sites and NH_3 molecules than between the Z2Cu sites and NH_3 molecules. Similar to the Cu/LTA sample, ZCuOH was the preferred adsorption site compared to Z2Cu for the Cu/SSZ-13 sample (Fig. 2**b**), however, this difference disappeared over time. The reason for this is suggested to be that the Cu/SSZ-13 sample used in the study contained a higher concentration of ZCuOH than Z2Cu, as shown in the H_2-TPR profiles (Fig. 1).

Following NH_3 adsorption (300 ppm NH_3, 10% O_2, balance Ar) and Ar purge for 20 min, NO (300 ppm NO, 10% O_2, balance Ar) was added to the feed gas. Fig. 2**a** and **b** (lower panels) display the DRIFTS spectra obtained during the reaction between NO and pre-adsorbed NH_3 with the Z2Cu and ZCuOH sites at 200 °C for Cu/LTA and Cu/SSZ-13, respectively. The adsorbed NH_3 was consumed gradually over time following the addition of 300 ppm NO to both Cu/zeolites, which was observed by the decrease in the two negative IR features at 900–930 and 950–960 cm^{-1} towards baseline [36]. This phenomenon confirms that both the ZCuOH and Z2Cu residing in the zeolites (i.e., LTA and CHA) were active for the NH_3-SCR reaction at 200 °C [33,61]. Although the overall trend was identical, a few key differences between the two types of zeolite were, nevertheless, found. First, slight negative bands were observed in both of the Cu/LTA and Cu/SSZ-13 samples after flowing in NO for 160 min. Specifically, solely one weak negative feature located at 950 cm^{-1} (i.e., ZCuOH) remained in the Cu/SSZ-13 sample, while the band at 900 cm^{-1} (i.e., Z2Cu) completely returned to baseline. This suggests that all the NH_3 adsorbed onto Z2Cu can react with NO, yet a very small portion of the NH_3 adsorbed onto ZCuOH cannot be consumed by NO, or the reaction rate is quite low at 200 °C. Moreover, it is worth noting that both of the negative bands of the Cu/LTA sample at 960 and 925 cm^{-1} partly remained, indicating that not only ZCuOH but also some Z2Cu did not readily function in the NH_3-SCR reaction at 200 °C for this sample. Therefore, based on the above results, we concluded that there is always a small amount of ZCuOH that cannot, or only slowly, participates in the SCR reaction, regardless if the sample is Cu/LTA or Cu/SSZ-13. However, some Z2Cu sites were not involved in the SCR reaction at 200 °C in the Cu/LTA sample. This could be due to either: (1) a portion of the Cu species being less active for an ammonia SCR reaction, or (2) the location of some Cu species, resulting in that not all species were accessible for NO after NH_3 adsorption, possibly due to steric hindrance [62].

To further confirm the distribution of Z2Cu and ZCuOH species for Cu/LTA and Cu/SSZ-13 samples with similar Cu/Al (~0.45) and Si/Al (~15) ratios, peak fittings were conducted to determine the relative area ratios of these two Cu ion species. The results are shown in Fig. 3 and listed in Table 2 together with the H_2-TPR results. Although DRIFTS cannot be used directly to quantify species, the results strongly support the H_2-TPR results (Fig. 1). It was also found that the concentration of ZCuOH in the Cu/SSZ-13 sample was significantly higher than the concentration in the Cu/LTA sample. Specifically, the ratio of Z2Cu to ZCuOH (i.e. the fraction of Z2Cu divided by the ZCuOH based on the H_2 TPR) was 7.3 (0.88/0.12) for the Cu/LTA sample, but only 0.54 (0.35/0.65) for the Cu/SSZ-13 sample. Note that the samples used in this study was pretreated at 750 °C for 4 h under standard SCR reaction conditions (400 ppm NO, 400 ppm NH_3, 5% H_2O, 10% O_2, 1200 ml/min) in the flow reactor. Therefore, it is expected that the content of ZCuOH will be higher in fresh Cu/SSZ-13 according to work from Gao et al. [33]. However, based on our previous work [35], the number of

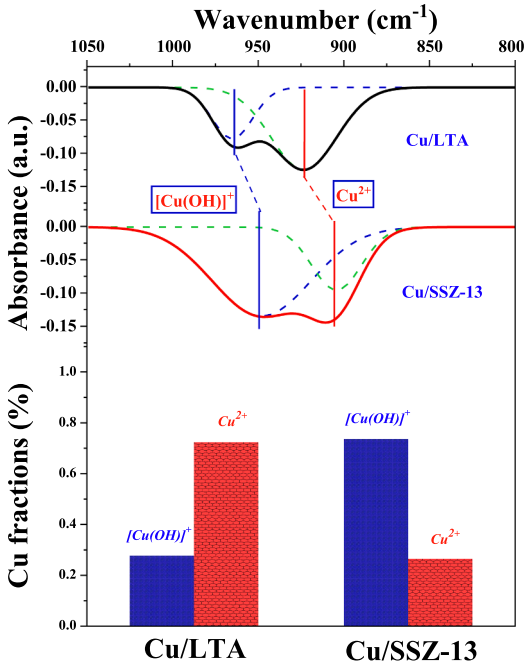

Fig. 3. Comparison of saturated DRIFTS spectra of T-O-T vibrational region perturbed by NH_3 adsorption for Cu/LTA and Cu/SSZ-13 samples with ZCuOH and Z2Cu populations.

Table 2
The fraction of different Cu species from DRIFTS and H_2-TPR for Cu/LTA and Cu/SSZ-13 samples.

Sample		ZCuOH	Z2Cu
Cu/LTA	DRIFTS	0.28	0.72
	H_2-TPR	0.12	0.88
Cu/SSZ-13	DRIFTS	0.73	0.27
	H_2-TPR	0.65	0.35

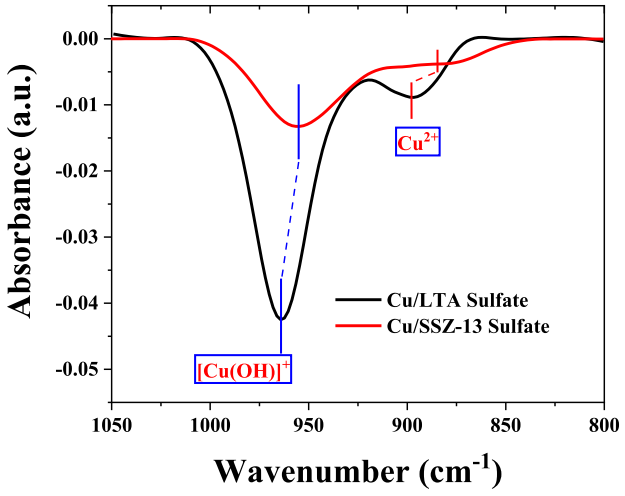

Fig. 4. DRIFTS spectra of T-O-T vibrational region perturbed by SO_2 poisoning for Cu/LTA (upper panel) and Cu/SSZ-13 (lower panel) samples.

ZCuOH in fresh Cu/LTA will be even lower, as we observed the gradual conversions of both Z2Cu and CuO_x clusters to ZCuOH with increasing aging temperature.

Fig. 4 presents the corresponding internal asymmetric T–O–T vibrations for the sulfated Cu/LTA and Cu/SSZ-13 samples (30 ppm SO_2,

10% O_2, balance Ar at 200 °C for 2 h) using the conditions prior to sulfation as background. Similar to the NH_3 pre-adsorption discussed above, the negative T–O–T vibration features mainly arose from perturbations induced by SO_2 interaction with isolated Cu ions residing close to the framework [36,59], i. e., ZCuOH and Z2Cu. Not surprisingly, two negative features were found at approximately 900–925 and 950–960 cm^{-1}, representing Z2Cu and ZCuOH for both Cu/zeolites. This indicates that SO_2 not only can interact with ZCuOH, as suggested in previous research [37,42,63], but can also interact somewhat with Z2Cu sites. However, it should be noted that interaction with Z2Cu sites was minor for both Cu/zeolites. Interestingly, Fig. 4 clearly shows that there was a significantly larger amount of sulfur adsorption onto the ion-exchanged Cu sites inside the Cu/LTA sample than inside the Cu/SSZ-13, especially at the ZCuOH sites. This was somewhat unexpected. As discussed above (Fig. 1 and Fig. 3), ZCuOH was the dominant Cu species in the Cu/SSZ-13 sample, while the majority of the copper in the Cu/LTA catalyst was Z2Cu. Considering that ZCuOH is commonly known to be more reactive with SO_2 [36,39,64], we would expect that the Cu/SSZ-13 sample would more readily interact with SO_2. However, this was not the case. It was found that ZCuOH sites in the Cu/LTA sample can adsorb more SO_2 despite the lower concentration. The results of the H_2-TPR method discussed earlier (Fig. 1) can reasonably explain this phenomenon. Since the ZCuOH in the Cu/LTA sample had a weaker interaction with the framework, as indicated by the lower reduction temperature, this makes Cu/LTA more susceptible to SO_2 poisoning than Cu/SSZ-13.

In addition, DRIFTS was also applied to examine the OH vibrational signals in the IR region at 3500–3800 cm^{-1} of the Cu/LTA and Cu/SSZ-13 samples after SO_2 poisoning. Fig. 5 depicts the sulfated samples with well-resolved negative/positive bands by using the clean catalyst surface as the background. After SO_2 poisoning, the Cu/LTA and Cu/SSZ-13 samples showed consistent features, i.e., 3734/3735, 3708/3715, 3678/3683, 3650/3654, 3608/3612, and 3564/3582 cm^{-1}. The 3734/3735 cm^{-1} and 3708/3715 cm^{-1} bands can be attributed to the impact of sulfur on isolated and vicinal Si-OH sites, respectively, and the 3678/3683 cm^{-1} bands can be attributed to external Al-OH sites. The bands at 3564 and 3612 cm^{-1} in the Cu/LTA sample are assigned to Brønsted

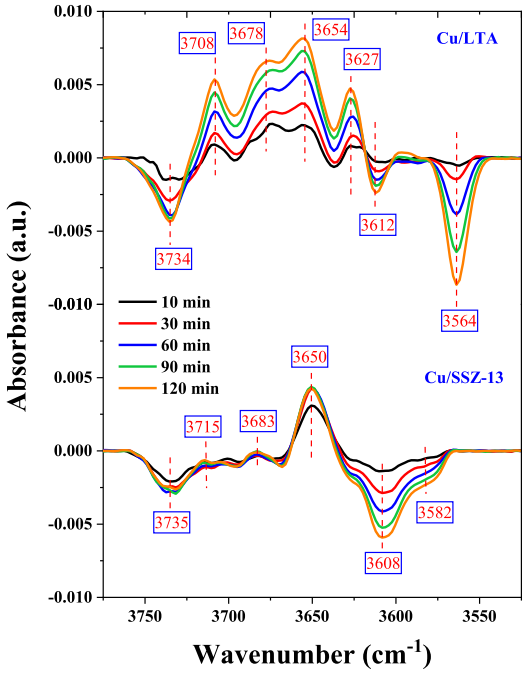

Fig. 5. DRIFTS spectra of the OH vibrational region caused by SO_2 poisoning of the Cu/LTA and Cu/SSZ-13 samples.

acid sites, i.e., Al-OH-Si, where the corresponding bands were 3582 and 3608 cm^{-1} for the Cu/SSZ-13 sample. Note here although our Cu/Al ratios were near saturation, i.e., close to 0.5, as shown in Table 1 for the two samples, the intensity of the Brønsted acid sites remained strong. This again confirms the presence of monovalent copper complexes, i.e., ZCuOH, with only one framework Al needed for a charge balance. The reason is that if all the Cu was in the form of Z2Cu, each Cu would need two framework Al, which would consume all the Brønsted acid sites. Since we observe Brønsted acid sites remaining, not all Cu can be in Z2Cu form, thus ZCuOH are also present. Moreover, the bands at 3650/3654 cm^{-1} can most likely be attributed to the Cu-OH species [33]. First of all, it is worth mentioning that regardless of whether a peak is positive or negative, it is caused by the effect of SO_2 interaction, since only SO_2 and O_2 are present. Therefore, our results show that in Cu/SSZ-13, only Brønsted acid sites (i.e., Al-OH-Si), Cu-OH and Si-OH were able to interact with SO_2. However, the interactions of sulfur with the framework were found to be weak for the Cu/SSZ-13 sample.

Interestingly, a large amount of –OH groups in the Cu/LTA sample were found to be significantly affected by SO_2. Especially, in the case of 3650/3654 cm^{-1}, corresponding to Cu-OH sites, the intensity of the Cu/LTA sample was much stronger than that of Cu/SSZ-13. This is in line with the results displayed in Fig. 4. Once again, this confirms that the ZCuOH in the Cu/LTA sample was more susceptible to SO_2 poisoning. Moreover, the intensity of Brønsted acid sites in Cu/TLA catalyst (i.e., 3564 cm^{-1}) was stronger than that of Cu/SSZ-13 catalyst (i.e., 3608 cm^{-1}) from Fig. 5. This was most likely due to the stronger interaction between Al-OH-Si and SO_2 in Cu/LTA.

3.3. SO_2 temperature-programmed desorption (SO_2-TPD) results

Cu/LTA and Cu/SSZ-13 samples were treated with SO_2 at 250 °C for sulfur deposition under three conditions (i.e., SO_2, SO_2 + H_2O, and SO_2 + NH_3 + H_2O) to gain insight into differences in the SO_2 poisoning of Cu/LTA and Cu/SSZ-13 samples and to understand the influence of the addition of NH_3 and H_2O. The TPD results are shown in Fig. 6. The SO_2 desorption signals of the Cu/zeolites were integrated to quantify the extent of sulfation under different SO_2 poisoning conditions, shown as mmol/$g_{washcoat}$. The values are presented with inserts in the upper-left corners of the figures and are listed in Table 3.

Only one high-temperature desorption state (> 600 °C) was found for the Cu/LTA and Cu/SSZ-13 samples under dry conditions with only SO_2 present, which was due to the decomposition of copper sulfate species [36,46,65], see Fig. 6 (orange line). Note that the S_{High}/ZCuOH ratios have also been calculated and are listed in Table 3, where S_{High} represents the amount of SO_2 desorption at high temperature (> 600 °C), and the value of ZCuOH was obtained based on the ICP (Table 1) and H_2-TPR results (Fig. 1). As confirmed by DRIFTS data (Fig. 4), ZCuOH is significantly more vulnerable to SO_2 than Z2Cu. Thus, using the S_{High}/ZCuOH ratio is reasonable since the majority of the formed copper sulfate should be from ZCuOH. The ratio of S_{High}/ZCuOH derived from the Cu/LTA sample (0.64) in the presence of SO_2 only is a factor of 10 times larger than the ratio in the Cu/SSZ-13 sample (0.06). This result is consistent with the DRIFTS data (Fig. 4 and Fig. 5) and H_2-TPR results (Fig. 1), where the ZCuOH sites residing in the Cu/LTA sample were found to be more susceptible to SO_2 due to weaker binding energy with the framework.

One key feature found for both Cu/zeolites was that H_2O greatly enhances the formation of stable sulfur species (copper sulfate), as shown in the TPD curves (green line), which decompose at high temperature, i.e., above 600 °C. This finding is consistent with the work by Wijayanti et al. [46]. It should be noted that some H_2SO_4 can be formed in the presence of H_2O, which is difficult to detect in our reactor system. However, this is only a small amount (ca 10%) based on our adsorption and desorption mass balance calculations and will not affect the trend. Therefore, here, the TPD results suggest that in the presence of H_2O, ZCuOH is interacting with H_2O, leading to a dramatic increase in SO_2

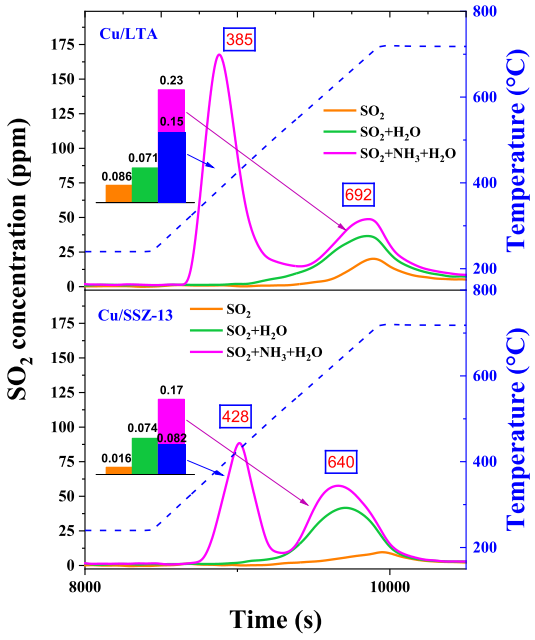

Fig. 6. SO_2-TPD profiles for Cu/LTA (upper panels) and Cu/SSZ-13 (lower panels) samples after adsorption with (1) 30 ppm SO_2, 10% O_2, balance with Ar (named as SO_2); (2) 30 ppm SO_2, 5% H_2O, 10% O_2, balanced with Ar (named as SO_2 + H_2O); (3) 30 ppm SO_2, 5% H_2O, 400 ppm NH_3, 10% O_2, balanced with Ar (named as SO_2 + NH_3 + H_2O).

storage for both Cu/zeolites. In this case, the S_{High}/ZCuOH ratio of Cu/LTA is ca 1.31, which is even higher than 1. This should indicate that almost all of the ZCuOH in the Cu/LTA sample was poisoned by sulfur in the presence of H_2O. The part (~0.31) exceeding 1 may be due to some contribution from Z2Cu sites, as seen in the SO_2 DRIFTS experiments (Fig. 4). However, the ratio of S_{High}/ZCuOH in the Cu/SSZ-13 sample was only ~0.29, suggesting that many ZCuOH sites were not poisoned by sulfur in the presence of H_2O.

Next, NH_3 was added to the gas phase together with SO_2 and H_2O, as shown in Fig. 6 (pink line). Compared with the desorption curves of SO_2 only with/without H_2O, a new SO_2 desorption feature was observed at approximately 385 °C for the Cu/LTA sample and at 428 °C for the Cu/SSZ-13. This new feature is typically attributed to the decomposition of ammonium sulfate ($(NH_4)_2SO_4$) species [36,42]. Specifically, for the Cu/LTA sample, ~0.15 mmol/$g_{washcoat}$ was from ammonium sulfates, and the corresponding value for the Cu/SSZ-13 sample was ~0.06 mmol/$g_{washcoat}$. Significantly more ammonium sulfates were formed in the Cu/LTA sample. It is known that the cage size of the LTA structure (12.3 Å × 12.3 Å × 12.3 Å) is significantly larger than that of CHA structure (10.9 Å × 6.7 Å × 9.4 Å) [57]. This may also contribute to the formation of more ammonium sulfates in Cu/LTA. The presence of NH_3 can promote the formation of copper sulfate species to a certain extent since some of the ammonium sulfates can be transformed into copper sulfates during the TPD ramp [46].

3.4. NH_3 temperature-programmed desorption (NH_3-TPD) results

Brønsted and Lewis acid sites were investigated using NH_3-TPD experiments. The formation and decomposition of ammonium sulfate were further studied using NH_3/SO_2-TPD experiments. NH_3 desorption results are presented in Fig. 7**a** and **b** (upper panels) for the Cu/LTA and Cu/SSZ-13 samples, respectively, for two NH_3 adsorption conditions, i.e., NH_3 + H_2O and NH_3 + SO_2 + H_2O. Two main NH_3 desorption states were found for both Cu/LTA and Cu/SSZ-13 samples without SO_2 during adsorption (black line in the upper panels of Fig. 7): a low-temperature feature at ~200 °C, and a high-temperature feature at ~300 °C. According to previous studies [53,66], the peak at 200 °C is mainly attributed to the desorption of NH_3 from ion-exchanged Cu sites. The high-temperature peak (i.e., 300 °C) is attributed to the desorption of NH_3 from Brønsted acid sites and also partly to the contribution from NH_3 stored on strong Lewis acid sites, i.e., ion-exchanged Cu sites [35]. Interestingly, the capacities for NH_3 storage were greatly improved through all temperature regions in the presence of SO_2 in the adsorption feed gas (red line in the upper panels of Fig. 7).

The increase in NH_3 storage can be attributed to: (1) the newly generated acidic sites, and/or (2) the decomposition of produced ammonium sulfates. New acidic sites occur because some of the anchoring S atoms can be associated with the more acidic hydroxyl group in the form of S-OH, which facilitates a relatively strong coordination binding between the NH_3 molecule and such acidic sites. A similar phenomenon has also been found in phosphorus-poisoned Cu/SSZ-13 samples [11]. Therefore, the subtracted curves (i.e., the TPD curve with SO_2 (red line) minus that without SO_2 (black line)) are also presented in Fig. 7**a** and **b** (lower panels) for a more intuitive and clear understanding of the changes to the desorption of NH_3 after the addition of SO_2. Peak fittings were used to quantify the amount of newly generated NH_3 desorption states after the addition of SO_2 for these two Cu/zeolites. The obtained results are listed in Table 4 together with the amount of desorbed SO_2 that occurred as a result of the decomposition of $(NH_4)_2SO_4$ from SO_2-TPD (Fig. 6 and Table 3) for comparison. Note that these new features are denoted as T1 (190–210 °C), and T2 (360–390 °C), respectively.

First, it is worth to know that ammonium sulfates ($(NH_4)_2SO_4$) decompose upon heating above 250 °C, first forming ammonium bisulfate (NH_4HSO_4) and NH_3 (Equation (1)). Subsequently, higher temperatures result in further decomposition to N_2, NH_3, SO_2, and H_2O (Equation (2)) [67]. The decomposition reaction equations are as follows:

$$(NH_4)_2SO_4 \rightarrow NH_3 + NH_4HSO_4 \quad (1)$$

$$3NH_4HSO_4 \rightarrow NH_3 + N_2 + 3SO_2 + 6H_2O \quad (2)$$

$$3(NH_4)_2SO_4 \rightarrow 4NH_3 + 3SO_2 + 6H_2O + N_2 \quad (3)$$

Equation (3) is the overall decomposition process. Since $(NH_4)_2SO_4$ requires at least 250 °C to decompose, then T1 (190–210 °C) should be derived from the newly produced acid sites. T2 can possibly be attributed to the decomposition of $(NH_4)_2SO_4$, where two steps (Equation (1) and (2)) overlap in the T2 region. Regarding T1, more new acid sites were formed in the Cu/LTA sample than in the Cu/SSZ-13, with the

Table 3
SO_2 storage (mmol/$g_{washcoat}$) and S_{High}/ZCuOH ratios of different adsorption conditions for Cu/LTA and Cu/SSZ-13 samples.

Samples	SO_2			SO_2 + H_2O			SO_2 + NH_3 + H_2O		
	Storage (mmol/$g_{washcoat}$)		S_{High}/ZCuOH ratio	Storage (mmol/$g_{washcoat}$)		S_{High}/ZCuOH ratio	Storage (mmol/$g_{washcoat}$)		S_{High}/ZCuOH ratio
	Low	High		Low	High		Low	High	
Cu/LTA	0	0.035	0.64	0	0.071	1.31	0.15	0.086	1.59
Cu/SSZ-13	0	0.015	0.06	0	0.074	0.29	0.062	0.093	0.37

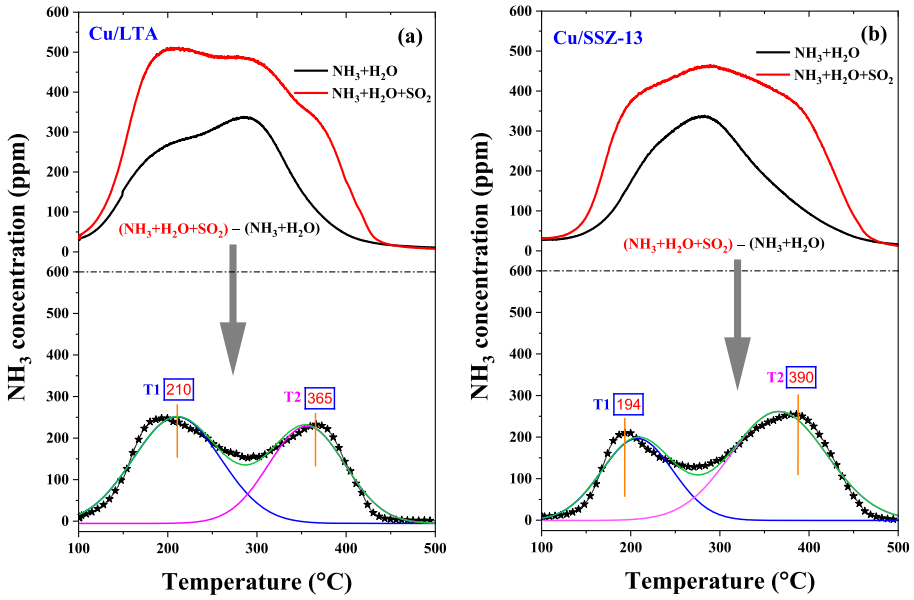

Fig. 7. NH_3-TPD profiles for (a) the Cu/LTA sample (upper panel) and (b) the Cu/SSZ-13 sample (upper panel) under two feed conditions (i.e., NH_3 + H_2O and NH_3 + SO_2 + H_2O); and the subtracted curves of (a) Cu/LTA (lower panel) and (b) Cu/SSZ-13 (lower panel) from these two condition curves.

Table 4
Newly formed NH_3 storage (mmol/$g_{washcoat}$) of two desorption states (i.e., T1 and T2) for the Cu/LTA and Cu/SSZ-13 samples.

Temperature (°C)	T1 (mmol/$g_{washcoat}$)	T2 (mmol/$g_{washcoat}$)	SO_2 storage (Low-temp) (mmol/$g_{washcoat}$)
Cu/LTA	0.24	0.19	0.15
Cu/SSZ-13	0.16	0.29	0.062

values of 0.24 and 0.16 mmol/$g_{washcoat}$, respectively.

To confirm our proposal that T2 occurs from the decomposition of ammonium sulfates, and also according to Equation (3), it is clear that the total ratio of generated NH_3 and SO_2 upon $(NH_4)_2SO_4$ decomposition is 4 to 3. Therefore, it was interesting to compare the values of NH_3 storage (T2) from NH_3-TPD multiplied by a factor of 3 and SO_2 storage due to the decomposition of ammonium sulfate from SO_2-TPD, multiplied by a factor of 4. The results are calculated and plotted in Fig. 8. Interestingly, the two values were highly identical for the Cu/LTA sample, suggesting that the T2 of Cu/LTA can mainly be attributed to the decomposition of $(NH_4)_2SO_4$. However, regarding Cu/SSZ-13, the value of 'NH_3(T2) × 3' was much higher than that of 'SO_2 (Low-temp) × 4'. This indicates that the desorption of NH_3 (T2) from the Cu/SSZ-13 sample cannot only be attributed to the decomposition of ammonium sulfates but also to some NH_3 desorbed from other sources, such as newly formed acidic sites that are stronger than T1, and/or some SO_2 that had not desorbed but directly converted to copper sulfate. As discussed in the SO_2-TPD section, some of the ammonium sulfate had transformed to copper sulfates during the TPD ramp, however, the amount was limited, with only ~0.02 mmol/$g_{washcoat}$ for the Cu/SSZ-13 sample. Therefore, newly formed strong acidic sites in the T2 region is suggested to be the main explanation. Moreover, a slight delay in the desorption of SO_2 (Fig. 6) occurred after the decomposition of ammonium sulfate in comparison with the release of NH_3 (Fig. 7), i.e., the temperatures were 365 °C (390 °C) with NH_3 and 385 °C (428 °C) with SO_2 desorption for the Cu/LTA (Cu/SSZ-13) samples, respectively.

3.5. Reaction results

SO_2 poisoning was conducted under standard SCR reaction conditions. As displayed in Fig. 9, the catalysts were first heated from room temperature to 250 °C and were maintained at this temperature for 0.5 h under standard SCR conditions (400 ppm NO, 400 ppm NH_3, 10% O_2, 5% H_2O and balance Ar). Thereafter, 30 ppm SO_2 was doped into the feed gas for 2 h, followed by a purge in the SCR gas again for 0.5 h (SO_2 was turned off). Cu/zeolites maintained high catalytic activity prior to the addition of SO_2. The activity of the sample began to descend immediately after the addition of SO_2 to the reaction gas. We found that the breakthrough of SO_2 in the Cu/LTA sample (green line) was slower than in the Cu/SSZ-13 (orange line). This indicates that the Cu/LTA sample was able to store more SO_2, which is consistent with the SO_2-TPD results. The calculated values of the SO_2 storage are inserted in Fig. 9, 0.24 and 0.17 mmol/$g_{washcoat}$ for the Cu/LTA and Cu/SSZ-13 samples, respectively. This is similar to the amount desorbed from SO_2-TPD (0.23 and 0.16 mmol/$g_{washcoat}$, Fig. 6). It is clear that more than 95% of stored SO_2 in the catalyst was released and only minor amount (5% or less) of sulfur might remain after the TPD.

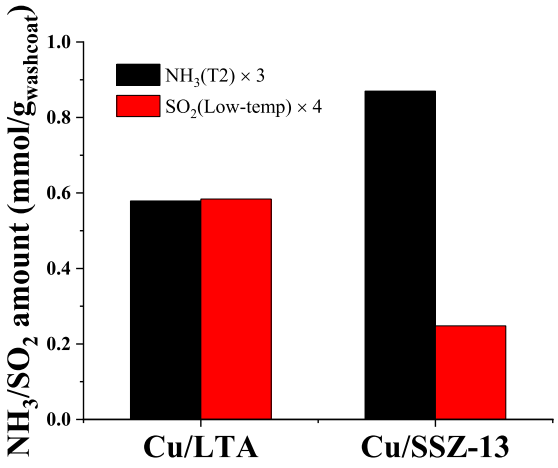

Fig. 8. A comparison of NH_3 storage (T2, mmol/$g_{washcoat}$) × 3 and SO_2 storage from $(NH_4)_2SO_4$ decomposition (mmol/$g_{washcoat}$) × 4 for Cu/LTA and Cu/SSZ-13.

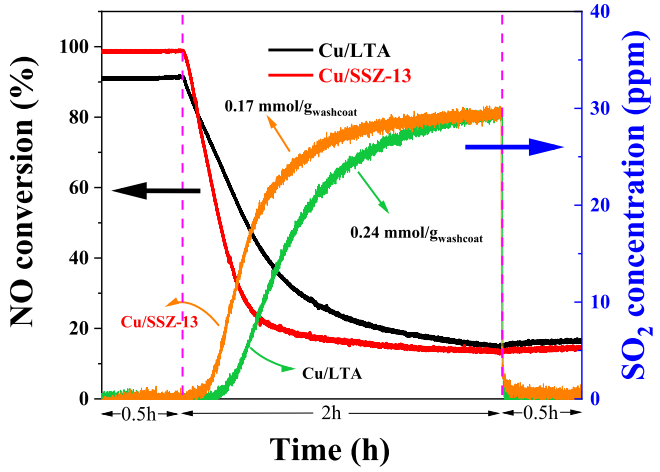

Fig. 9. NO conversions of standard SCR reaction during SO_2 poisoning at 250 °C for Cu/LTA and Cu/SSZ-13 samples. The reactant feed contained 400 ppm NO, 400 ppm NH_3, 30 ppm SO_2 (if needed), 10% O_2, 5% H_2O balanced with Ar at a GHSV of 22,100 h^{-1}.

Interestingly, it was observed that the rate of decline in the catalytic activity of the two Cu/zeolites was different. The deactivation rate of the Cu/LTA sample was significantly slower than that of the Cu/SSZ-13. This seems to contradict the results above, which show that the Cu/LTA sample can store more SO_2 than the Cu/SSZ-13, where the Cu/LTA catalyst was expected to be easier to deactivate through SO_2 poisoning. However, this is not the case here. According to the SO_2-TPD results discussed above, under SO_2 + NH_3 + H_2O condition, even though the S_{High}/ZCuOH ratio of the Cu/LTA sample (1.59) was much higher than for the Cu/SSZ-13 (0.37), however, the actual values of poisoned ZCuOH sites were basically the same, 0.086 and 0.093 mmol/$g_{washcoat}$, respectively. Therefore, the key factor for deactivation should be the formation of ammonium sulfates, especially where they are located. The SO_2-TPD results (Fig. 6) suggest that more ammonium sulfates were formed in the Cu/LTA sample, and according to the DRIFTS data (Fig. 5), it is clear that large amount of –OH groups (e.g., external Al-OH sites) in the Cu/LTA sample can interact with SO_2, therefore, it is reasonable that more ammonium sulfates would be formed on these –OH groups, which would not affect SCR activity significantly. However, fewer framework –OH groups in the Cu/SSZ-13 sample were associated with SO_2, and more important is that still plently of ZCuOH sites were not converted to copper sulfate (S_{High}/ZCuOH ~ 0.37). It is believed that $(NH_4)_2SO_4$ would preferably attach to these unconverted ZCuOH sites, which would seriously affect SCR activity. Thus, the slow deactivation of the Cu/LTA sample is reasonable due to the diversity of the locations of $(NH_4)_2SO_4$.

Fig. 10**(a)** and **(c)** depict the standard NH_3-SCR ($4NH_3 + 4NO + O_2 \rightarrow 4\,N_2 + 6H_2O$) light-off curves of NO_x for fresh, sulfated, and regenerated (400, 500, 600, and 750 °C) Cu/LTA and Cu/SSZ-13 samples, respectively. The SO_2 poisoning process of the sulfated samples is described in detailed in the previous paragraph. Following this process, the sulfate samples were continuously regenerated at 400, 500, 600, and 750 °C in 10% O_2/Ar for 2 h. Noteworthy, for fresh samples, regardless whether the reactions were standard or fast SCR, Cu/SSZ-13 experienced a more severe selectivity decline than Cu/LTA at high temperature. The NO_x conversion of the Cu/SSZ-13 sample was reduced by 40% (from 100% at 400 °C to 60% at 550 °C) for the fast SCR reaction, which is almost twice the reduction in conversion for the Cu/LTA sample (from 100% at 400 °C to 80% at 550 °C). As we know, the presence of CuO_x clusters in Cu/zeolites is typically claimed to be responsible for the subsequent decline in catalyst selectivity at high reaction temperatures due to ammonia oxidation [33,68].

Another difference between fresh Cu/LTA and Cu/SSZ-13 samples that deserves attention is the low-temperature catalytic activity for standard and fast SCR reactions. Briefly, the performance of the Cu/SSZ-13 sample was better than the performance of the Cu/LTA in the low-temperature interval for the standard SCR reaction. This is in line with the DRIFTS results shown in Fig. 2, where both Cu active sites are less reactive to NO + NH_3 reaction in Cu/LTA as compared to Cu/SSZ 13. However, the performance of these two samples were similar for fast SCR reactions [35,60]. For example, at 175 and 200 °C of standard SCR reaction, the NO_x conversions of the Cu/LTA catalyst were 22% and 45%, respectively, while the NO_x conversions of the Cu/SSZ-13 were 38% and 71%, respectively. However, in fast SCR reaction, the conversions were 80% and 75% (175 °C) for the Cu/LTA and CuSSZ-13 samples, respectively, i.e., a fast SCR reaction is less sensitive to the type of Cu species used. There are several possible reasons for this difference in standard SCR reaction, such as: (1) the zeolite framework structure diversity between LTA and CHA; (2) the difference in ZCuOH and Z2Cu population, i.e. ZCuOH and Z2Cu are dominant in Cu/SSZ-13 and Cu/LTA, respectively; (3) the location of some Cu species in the Cu/LTA sample, that are not accessible for NO after the adsorption of NH_3, according to the DRIFTS results (Fig. 2). This is possibly due to steric hindrance. Regarding point (1), we examined standard and fast SCR reactions for H/LTA and H/SSZ-13 (not shown). No significant difference was found between H/LTA and H/SSZ-13. Therefore, we can rule out the reason (1).

Regarding SO_2 poisoning, both of the sulfated Cu/zeolites (red lines in Fig. 10) experienced a certain degree of deactivation, regardless of whether a standard or a fast SCR reaction was used. The loss in the conversion of NO_x during standard and fast SCR reactions for the Cu/LTA and Cu/SSZ-13 samples is calculated and displayed in Fig. 11. As shown in the figure, the Cu/LTA sample dropped less in the standard SCR reaction than the CuSSZ-13 catalyst, but instead decreased more in the fast SCR reaction. Regarding standard SCR, the reason for this difference may just be as simple as the activity of fresh Cu/LTA is less, then the decline seems less, as the activities of sulfated catalysts are similar. However, the reason for standard SCR does not apply to fast SCR. Here, we propose that ZCuOH may be more active for fast SCR reactions, where ZCuOH in the Cu/LTA sample has been fully poisoned.

As the regeneration temperature increased, the activity of the samples gradually recovered. One interesting phenomenon of the Cu/SSZ-13 sample is that after regeneration at 600 °C (orange lines), its high temperature performance was even better than the fresh sample in both standard and fast SCR reactions. This was not found for the Cu/LTA sample, and we suggest that this is related to the CuO_x clusters in the sample. Briefly, as we know, CuO_x clusters can also interact with SO_2 to form copper sulfate species, and the required decomposition temperature is approximately 650–700 °C [36,42], which we also observed in the SO_2-TPD profiles (Fig. 6). Therefore, these copper sulfate species are stable after regeneration at 600 °C, which hinders the non-selective oxidation of NH_3 by CuO_x clusters in the Cu/SSZ-13 sample. However, as our group and Jo et al. [35,57] have suggested, the CuO_x clusters in the Cu/LTA sample contribute little to the non-selective oxidation of NH_3, thus, it is reasonable that similar phenomena would not be observed. This further confirms the various oxidation properties of the CuO_x clusters in these two Cu/zeolites.

Finally, upon regeneration at 750 °C, the Cu/LTA catalyst was restored to its original catalytic activity over the full temperature range (150–550 °C) in both standard and fast SCR reactions. However, low temperature activity was fully recovered in the Cu/SSZ-13 sample, but high temperature activity experienced a certain degree of loss in the two SCR reactions. The results suggest that the physical and chemical properties of the Cu/LTA sample had essentially recovered, whereas some negative changes occurred in the Cu/SSZ-13 sample after regeneration at 750 °C. We must emphasize here that, prior to using fresh Cu/LTA and Cu/SSZ-13, they were degreened at 750 °C for 4 h under the reaction condition (400 ppm NO, 400 ppm NH_3, 5% H_2O, 10% O_2 with Ar). Thus, regeneration at 750 °C for 2 h, especially under dry

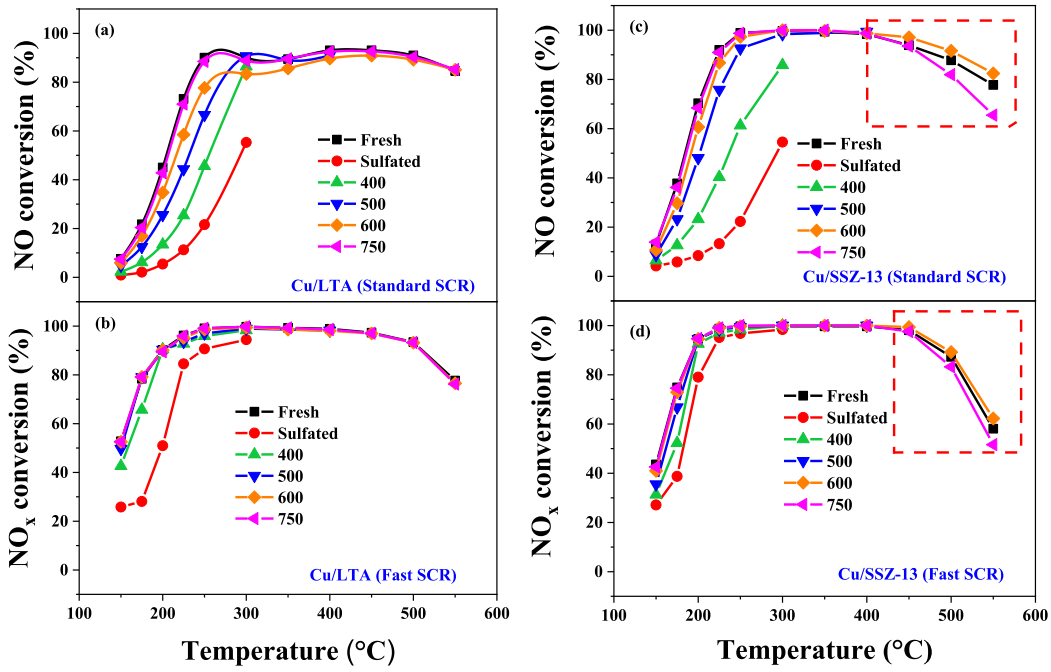

Fig. 10. (a), (c) NO conversion as a function of temperature during standard NH_3-SCR, and (b), (d) NO_x conversion as a function of temperature during fast NH_3-SCR for fresh, sulfated, and different temperature-regenerated (400, 500, 600, and 750 °C) Cu/LTA and Cu/SSZ-13 samples. The reactant feed contained 400 ppm NO (or 200 ppm NO and 200 ppm NO_2 for fast SCR), 400 ppm NH_3, 10% O_2, 5% H_2O balanced with Ar at a GHSV of 22,100 h^{-1}.

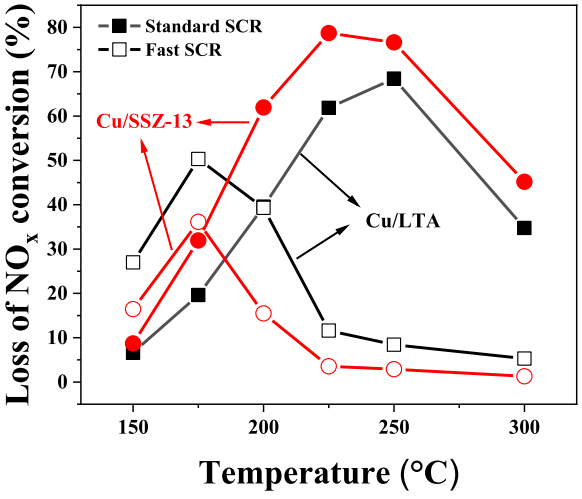

Fig. 11. Loss in conversion of NO_x in standard SCR (solid symbols) and fast SCR (hollow symbols) reactions over the Cu/LTA (black lines) and Cu/SSZ-13 (red lines) samples after sulfur poisoning. (For interpretation of the references to color in this figure legend, the reader is referred to the web version of this article.)

conditions (10% O_2/Ar), is not supposed to cause any structural degradation of either of the samples, Cu/LTA or Cu/SSZ-13 (Si/Al ~ 15). The most likely explanation for the high temperature activity loss of the Cu/SSZ-13 sample is that when copper sulfate species decompose at 750 °C [45,46], a small amount of new CuO_x clusters are produced simultaneously as the CuO_x clusters in the fresh catalyst are restored. The newly formed CuO_x clusters are considered to be the former isolated Cu ions at the ion exchange site, i.e., ZCuOH and/or Z2Cu, which were detached from the framework during the desulfurization process at 750 °C.

4. Conclusions

Two model catalysts, i.e., Cu/LTA and Cu/SSZ-13, with similar Si/Al and Cu/Al ratios were synthesized using the incipient wetness impregnation (IWI) method. Fresh, sulfated, and different temperature-regenerated (400, 500, 600, and 750 °C) samples were used to study the effect of SO_2 poisoning and regeneration for standard and fast SCR reactions. A number of characterization methods, including *in-situ* DRIFTS, H_2-TPR, various NH_3-TPD and SO_2-TPD, were used to obtain insight into the catalytic deactivation mechanism upon the sulfur poisoning of Cu/LTA and Cu/SSZ-13 samples.

Both samples contained multiple Cu-containing species, including ion-exchanged ZCuOH, Z2Cu sites, and a small amount of CuO_x clusters. Note that the Cu/SSZ-13 sample contained a higher concentration of ZCuOH than the Cu/LTA at similar Cu loadings. This also reflects the difference in the distribution of Al in the two zeolites; more of the Al sites in LTA are located nearby each other. We found that SO_2 more readily interacts with ZCuOH sites than with Z2Cu sites, which is in line with previous research. However, surprisingly, the ZCuOH in the Cu/LTA sample was found to be much more vulnerable to SO_2 poisoning than the Cu/SSZ-13, due to its lower binding energy with the framework. Moreover, SO_2-TPD results show that the presence of H_2O significantly increased sulfur storage. NH_3-TPD results suggest that the presence of SO_2 can contribute to generate new acidic sites that can adsorb NH_3, where for Cu/LTA is only at low temperature (T1), but for Cu/SSZ-13, both at low (T1) and high temperature (T2).

Under NH_3-SCR reaction conditions in the presence of SO_2, the Cu/LTA sample stored much more SO_2 than the Cu/SSZ-13, and it also had a slower deactivation rate than the Cu/SSZ-13 sample. The additional SO_2 storage in the Cu/LTA sample was found to be ammonium sulfates, because a large amount of the –OH groups in the sample could interact with SO_2. Moreover, the $(NH_4)_2SO_4$ in the Cu/SSZ-13 sample is believed to preferably attach to the ZCuOH sites that have not transferred to copper sulfate, which results in a faster deactivation rate.

The impact of the CuO_x clusters on the Cu/LTA sample on high temperature selectivity was confirmed to be significantly less than the

impact on the Cu/SSZ-13 sample. In addition, SO_2 poisoning was proved to be able to hinder the non-selective oxidation of NH_3 by CuO_x clusters for Cu/SSZ-13 sample regenerated at 600 °C. Upon regeneration at 750 °C, the Cu/LTA sample could be restored to its original catalytic activity over the full temperature range (150–550 °C) in both standard and fast SCR reactions. However, in terms of Cu/SSZ-13, the low-temperature activity was fully recovered, but high-temperature activity experienced a certain degree of loss in the two SCR reactions. This loss was mainly due to the formation of new CuO_x clusters. This further confirms that the Cu/LTA is a robust catalyst with good potential as an SCR catalyst not only towards hydrothermal aging but also towards sulfur poisoning and regeneration.

Declaration of Competing Interest

The authors declare that they have no known competing financial interests or personal relationships that could have appeared to influence the work reported in this paper.

Acknowledgements

This study was performed at the Division of Chemical Engineering and the Competence Centre for Catalysis, Chalmers University of Technology. The authors gratefully acknowledge financial support from the Swedish Research Council (642-2014-5733) and the Area of Advance Transport at Chalmers University of Technology. We would also like to acknowledge Prof. Suk Bong Hong and Dr Donghui Jo at Pohang University of Science and Technology (POSTECH) for helpful advice regarding LTA synthesis.

References

[1] A. Wang, L. Olsson, The impact of automotive catalysis on the United Nations sustainable development goals, Nat. Catal. 2 (2019) 566–570, https://doi.org/10.1038/s41929-019-0318-3.
[2] G.L. Chiarello, D. Ferri, J.-D. Grunwaldt, L. Forni, A. Baiker, Flame-synthesized $LaCoO_3$-supported Pd: 2. Catalytic behavior in the reduction of NO by H_2 under lean conditions, J. Catal. 252 (2007) 137–147, https://doi.org/10.1016/j.jcat.2007.10.003.
[3] H. Hamada, M. Haneda, A review of selective catalytic reduction of nitrogen oxides with hydrogen and carbon monoxide, Appl. Catal. A-Gen. 421–422 (2012) 1–13, https://doi.org/10.1016/j.apcata.2012.02.005.
[4] T. Nakatsuji, T. Yamaguchi, N. Sato, H. Ohno, A selective NO_x reduction on Rh-based catalysts in lean conditions using CO as a main reductant, Appl. Catal. B-Environ. 85 (2008) 61–70, https://doi.org/10.1016/j.apcatb.2008.06.024.
[5] F. Lónyi, J. Valyon, L. Gutierrez, M.A. Ulla, E.A. Lombardo, The SCR of NO with CH_4 over Co- Co, Pt-, and H-mordenite catalysts, Appl. Catal. B-Environ. 73 (2007) 1–10, https://doi.org/10.1016/j.apcatb.2006.11.017.
[6] M. Moreno-González, A.E. Palomares, M. Chiesa, M. Boronat, E. Giamello, T. Blasco, Evidence of a Cu^{2+}–alkane interaction in Cu-zeolite catalysts crucial for the selective catalytic reduction of NO_x with hydrocarbons, ACS Catal. 7 (2017) 3501–3509, https://doi.org/10.1021/acscatal.6b03473.
[7] P. Vernoux, A.Y. Leinekugel-Le-Cocq, F. Gaillard, Effect of the addition of Na to Pt/Al_2O_3 catalysts for the reduction of NO by C_3H_8 and C_3H_6 under lean-burn conditions, J. Catal. 219 (2003) 247–257, https://doi.org/10.1016/S0021-9517(03)00200-8.
[8] A. Wang, Y. Chen, E.D. Walter, N.M. Washton, D. Mei, T. Varga, Y. Wang, J. Szanyi, Y. Wang, C.H.F. Peden, F. Gao, Unraveling the mysterious failure of Cu/SAPO-34 selective catalytic reduction catalysts, Nat. Commun. 10 (2019) 1137, https://doi.org/10.1038/s41467-019-09021-3.
[9] A. Marberger, A.W. Petrov, P. Steiger, M. Elsener, O. Krocher, M. Nachtegaal, D. Ferri, Time-resolved copper speciation during selective catalytic reduction of NO on Cu-SSZ-13, Nat. Catal. 1 (2018) 221–227, https://doi.org/10.1038/s41929-018-0032-6.
[10] F. Gao, D.H. Mei, Y.L. Wang, J. Szanyi, C.H.F. Peden, Selective catalytic reduction over Cu/SSZ-13: linking homo- and heterogeneous catalysis, J. Am. Chem. Soc. 139 (2017) 4935–4942, https://doi.org/10.1021/jacs.7b01128.
[11] K. Xie, A. Wang, J. Woo, A. Kumar, K. Kamasamudram, L. Olsson, Deactivation of Cu-SSZ-13 SCR catalysts by vapor-phase phosphorus exposure, Appl. Catal. B-Environ. 256 (2019) 117815, , https://doi.org/10.1016/j.apcatb.2019.117815.
[12] X. Li, K. Li, Y. Peng, X. Li, Y. Zhang, D. Wang, J. Chen, J. Li, Interaction of phosphorus with a $FeTiO_x$ catalyst for selective catalytic reduction of NO_x with NH_3: Influence on surface acidity and SCR mechanism, Chem. Eng. J. 347 (2018) 173–183, https://doi.org/10.1016/j.cej.2018.04.035.
[13] G. He, Z. Lian, Y. Yu, Y. Yang, K. Liu, X. Shi, Z. Yan, W. Shan, H. He, Polymeric vanadyl species determine the low-temperature activity of V-based catalysts for the SCR of NO_x with NH_3, Sci. Advances 4 (2018) eaau4637, https://doi.org/10.1126/sciadv.aau4637.
[14] R.Q. Long, R.T. Yang, R. Chang, Low temperature selective catalytic reduction (SCR) of NO with NH_3 over Fe–Mn based catalysts, Chem. Commun. (2002) 452–453, https://doi.org/10.1039/B111382H.
[15] Y. Wan, W. Zhao, Y. Tang, L. Li, H. Wang, Y. Cui, J. Gu, Y. Li, J. Shi, Ni-Mn bi-metal oxide catalysts for the low temperature SCR removal of NO with NH_3, Appl. Catal. B-Environ. 148–149 (2014) 114–122, https://doi.org/10.1016/j.apcatb.2013.10.049.
[16] M.H. Zhu, J.K. Lai, U. Tumuluri, Z.L. Wu, I.E. Wachs, Nature of active sites and surface intermediates during SCR of NO with NH_3 by supported V_2O_5-WO_3/TiO_2 catalysts, J. Am. Chem. Soc. 139 (2017) 15624–15627, https://doi.org/10.1021/jacs.7b09646.
[17] X. Yao, L. Chen, J. Cao, Y. Chen, M. Tian, F. Yang, J. Sun, C. Tang, L. Dong, Enhancing the deNO_x performance of MnO_x/CeO_2-ZrO_2 nanorod catalyst for low-temperature NH_3-SCR by TiO_2 modification, Chem. Eng. J. 369 (2019) 46–56, https://doi.org/10.1016/j.cej.2019.03.052.
[18] P.S. Kim, M.K. Kim, B.K. Cho, I.S. Nam, S.H. Oh, Effect of H_2 on deNO_x performance of HC-SCR over Ag/Al_2O_3: morphological, chemical, and kinetic changes, J. Catal. 301 (2013) 65–76, https://doi.org/10.1016/j.jcat.2013.01.026.
[19] W.L. Johnson, G.B. Fisher, T.J. Toops, Mechanistic investigation of ethanol SCR of NO_x over Ag/Al_2O_3, Catal. Today 184 (2012) 166–177, https://doi.org/10.1016/j.cattod.2011.12.002.
[20] W. Wang, J.M. Herreros, A. Tsolakis, A.P.E. York, Increased NO_2 concentration in the diesel engine exhaust for improved Ag/Al_2O_3 catalyst NH_3-SCR activity, Chem. Eng. J. 270 (2015) 582–589, https://doi.org/10.1016/j.cej.2015.02.067.
[21] D. Wang, L. Zhang, K. Kamasamudram, W.S. Epling, In situ-DRIFTS study of selective catalytic reduction of NO_x by NH_3 over Cu-exchanged SAPO-34, ACS Catal. 3 (2013) 871–881, https://doi.org/10.1021/cs300843k.
[22] S.Y. Joshi, A. Kumar, J.Y. Luo, K. Kamasamudram, N.W. Currier, A. Yezerets, New insights into the mechanism of NH_3-SCR over Cu- and Fe-zeolite catalyst: apparent negative activation energy at high temperature and catalyst unit design consequences, Appl. Catal. B-Environ. 226 (2018) 565–574, https://doi.org/10.1016/j.apcatb.2017.12.076.
[23] N. Martin, C. Paris, P.N.R. Vennestrom, J.R. Thogersen, M. Moliner, A. Corma, Cage-based small-pore catalysts for NH_3-SCR prepared by combining bulky organic structure directing agents with modified zeolites as reagents, Appl. Catal. B-Environ. 217 (2017) 125–136, https://doi.org/10.1016/j.apcatb.2017.05.082.
[24] A. Wang, Y. Wang, E.D. Walter, R.K. Kukkadapu, Y. Guo, G. Lu, R.S. Weber, Y. Wang, C.H. Peden, F. Gao, Catalytic N_2O decomposition and reduction by NH_3 over Fe/Beta and Fe/SSZ-13 catalysts, J. Catal. 358 (2018) 199–210, https://doi.org/10.1016/j.jcat.2017.12.011.
[25] Y. Li, W. Song, J. Liu, Z. Zhao, M. Gao, Y. Wei, Q. Wang, J. Deng, The protection of CeO_2 thin film on Cu-SAPO-18 catalyst for highly stable catalytic NH_3-SCR performance, Chem. Eng. J. 330 (2017) 926–935, https://doi.org/10.1016/j.cej.2017.08.025.
[26] A.Y. Wang, Y.L. Wang, E.D. Walter, N.M. Washton, Y.L. Guo, G.Z. Lu, C.H.F. Peden, F. Gao, NH_3-SCR on Cu, Fe and Cu plus Fe exchanged beta and SSZ-13 catalysts: hydrothermal aging and propylene poisoning effects, Catal. Today 320 (2019) 91–99, https://doi.org/10.1016/j.cattod.2017.09.061.
[27] J. Wang, D. Fan, T. Yu, J. Wang, T. Hao, X. Hu, M. Shen, W. Li, Improvement of low-temperature hydrothermal stability of Cu/SAPO-34 catalysts by Cu^{2+} species, J. Catal. 322 (2015) 84–90, https://doi.org/10.1016/j.jcat.2014.11.010.
[28] C. Paolucci, I. Khurana, A.A. Parekh, S.C. Li, A.J. Shih, H. Li, J.R. Di Iorio, J.D. Albarracin-Caballero, A. Yezerets, J.T. Miller, W.N. Delgass, F.H. Ribeiro, W.F. Schneider, R. Gounder, Dynamic multinuclear sites formed by mobilized copper ions in NO_x selective catalytic reduction, Science 357 (2017) 898–903, https://doi.org/10.1126/science.aan5630.
[29] L. Chen, H. Falsig, T.V.W. Janssens, H. Gronbeck, Activation of oxygen on $(NH_3$-Cu-$NH_3)^{(+)}$ in NH_3-SCR over Cu-CHA, J. Catal. 358 (2018) 179–186, https://doi.org/10.1016/j.jcat.2017.12.009.
[30] C. Fan, Z. Chen, L. Pang, S.J. Ming, C.Y. Dong, K.B. Albert, P. Liu, J.Y. Wang, D.J. Zhu, H.P. Chen, T. Li, Steam and alkali resistant Cu-SSZ-13 catalyst for the selective catalytic reduction of NO_x in diesel exhaust, Chem. Eng. J. 334 (2018) 344–354, https://doi.org/10.1016/j.cej.2017.09.181.
[31] Y. Ma, S. Cheng, X. Wu, Y. Shi, L. Cao, L. Liu, R. Ran, Z. Si, J. Liu, D. Weng, Low-temperature solid-state ion-exchange method for preparing Cu-SSZ-13 selective catalytic reduction catalyst, ACS Catal. (2019) 6962–6973, https://doi.org/10.1021/acscatal.9b01730.
[32] E. Borfecchia, K. Lomachenko, F. Giordanino, H. Falsig, P. Beato, A. Soldatov, S. Bordiga, C. Lamberti, Revisiting the nature of Cu sites in the activated Cu-SSZ-13 catalyst for SCR reaction, Chem. Sci. 6 (2015) 548–563, https://doi.org/10.1039/C4SC02907K.
[33] J. Song, Y.L. Wang, E.D. Walter, N.M. Washton, D.H. Mei, L. Kovarik, M.H. Engelhard, S. Prodinger, Y. Wang, C.H.F. Peden, F. Gao, Toward rational design of Cu/SSZ-13 selective catalytic reduction catalysts: implications from atomic-level understanding of hydrothermal stability, ACS Catal. 7 (2017) 8214–8227, https://doi.org/10.1021/acscatal.7b03020.
[34] T. Ryu, N.H. Ahn, S. Seo, J. Cho, H. Kim, D. Jo, G.T. Park, P.S. Kim, C.H. Kim, E.L. Bruce, P.A. Wright, I.S. Nam, S.B. Hong, Fully copper-exchanged high-silica LTA zeolites as unrivaled hydrothermally stable NH_3-SCR catalysts, Angew. Chem. Int. Ed. 56 (2017) 3256–3260, https://doi.org/10.1002/anie.201610547.
[35] A. Wang, P. Arora, D. Bernin, A. Kumar, K. Kamasamudram, L. Olsson, Investigation of the robust hydrothermal stability of Cu/LTA for NH_3-SCR reaction, Appl. Catal. B-Environ. 246 (2019) 242–253, https://doi.org/10.1016/j.apcatb.2019.01.039.

[36] Y. Jangjou, Q. Do, Y.T. Gu, L.G. Lim, H. Sun, D. Wang, A. Kumar, J.H. Li, L.C. Grabow, W.S. Epling, Nature of Cu active centers in Cu-SSZ-13 and their responses to SO_2 exposure, ACS Catal. 8 (2018) 1325–1337, https://doi.org/10.1021/acscatal.7b03095.
[37] P.S. Hammershoi, Y. Jangjou, W.S. Epling, A.D. Jensen, T.V.W. Janssens, Reversible and irreversible deactivation of Cu-CHA NH_3-SCR catalysts by SO_2 and SO_3, Appl. Catal. B-Environ. 226 (2018) 38–45, https://doi.org/10.1016/j.apcatb.2017.12.018.
[38] K. Wijayanti, K. Leistner, S. Chand, A. Kumar, K. Kamasamudram, N.W. Currier, A. Yezerets, L. Olsson, Deactivation of Cu-SSZ-13 by SO_2 exposure under SCR conditions, Catal. Sci. Technol. 6 (2016) 2565–2579, https://doi.org/10.1039/c5cy01288k.
[39] A.J. Shih, I. Khurana, H. Li, J. González, A. Kumar, C. Paolucci, T.M. Lardinois, C.B. Jones, J.D. Albarracin Caballero, K. Kamasamudram, A. Yezerets, W.N. Delgass, J.T. Miller, A.L. Villa, W.F. Schneider, R. Gounder, F.H. Ribeiro, Spectroscopic and kinetic responses of Cu-SSZ-13 to SO_2 exposure and implications for NO_x selective catalytic reduction, Appl. Catal. A-Gen 574 (2019) 122–131, https://doi.org/10.1016/j.apcata.2019.01.024.
[40] Y.S. Cheng, C. Lambert, D.H. Kim, J.H. Kwak, S.J. Cho, C.H.F. Peden, The different impacts of SO_2 and SO_3 on Cu/zeolite SCR catalysts, Catal. Today 151 (2010) 266–270, https://doi.org/10.1016/j.cattod.2010.01.013.
[41] A. Kumar, M.A. Smith, K. Kamasamudram, N.W. Currier, H. An, A. Yezerets, Impact of different forms of feed sulfur on small-pore Cu-zeolite SCR catalyst, Catal. Today 231 (2014) 75–82, https://doi.org/10.1016/j.cattod.2013.12.038.
[42] L. Zhang, D. Wang, Y. Liu, K. Kamasamudram, J.H. Li, W. Epling, SO_2 poisoning impact on the NH_3-SCR reaction over a commercial Cu-SAPO-34 SCR catalyst, Appl. Catal. B-Environ. 156 (2014) 371–377, https://doi.org/10.1016/j.apcatb.2014.03.030.
[43] M.Q. Shen, H.Y. Wen, T. Hao, T. Yu, D.Q. Fan, J. Wang, W. Li, J.Q. Wang, Deactivation mechanism of SO_2 on Cu/SAPO-34 NH_3-SCR catalysts: structure and active Cu^{2+}, Catal. Sci. Technol. 5 (2015) 1741–1749, https://doi.org/10.1039/c4cy01129e.
[44] P.S. Hammershoi, P.N.R. Vennestrom, H. Falsig, A.D. Jensen, T.V.W. Janssens, Importance of the Cu oxidation state for the SO_2-poisoning of a Cu-SAPO-34 catalyst in the NH_3-SCR reaction, Appl. Catal. B-Environ. 236 (2018) 377–383, https://doi.org/10.1016/j.apcatb.2018.05.038.
[45] W.K. Su, Z.G. Li, Y.N. Zhang, C.C. Meng, J.H. Li, Identification of sulfate species and their influence on SCR performance of Cu/CHA catalyst, Catal. Sci. Technol. 7 (2017) 1523–1528, https://doi.org/10.1039/c7cy00302a.
[46] K. Wijayanti, K.P. Xie, A. Kumar, K. Kamasamudram, L. Olsson, Effect of gas compositions on SO_2 poisoning over Cu/SSZ-13 used for NH_3-SCR, Appl. Catal. B-Environ. 219 (2017) 142–154, https://doi.org/10.1016/j.apcatb.2017.07.017.
[47] J. Hun Kwak, H. Zhu, J.H. Lee, C.H.F. Peden, J. Szanyi, Two different cationic positions in Cu-SSZ-13? Chem. Commun. 48 (2012) 4758–4760, https://doi.org/10.1039/C2CC31184D.
[48] F. Gao, N.M. Washton, Y.L. Wang, M. Kollar, J. Szanyi, C.H.F. Peden, Effects of Si/Al ratio on Cu/SSZ-13 NH_3-SCR catalysts: implications for the active Cu species and the roles of Bronsted acidity, J. Catal. 331 (2015) 25–38, https://doi.org/10.1016/j.jcat.2015.08.004.
[49] J. Luo, D. Wang, A. Kumar, J. Li, K. Kamasamudram, N. Currier, A. Yezerets, Identification of two types of Cu sites in Cu/SSZ-13 and their unique responses to hydrothermal aging and sulfur poisoning, Catal. Today 267 (2016) 3–9, https://doi.org/10.1016/j.cattod.2015.12.002.
[50] B.W. Boal, J.E. Schmidt, M.A. Deimund, M.W. Deem, L.M. Henling, S.K. Brand, S.I. Zones, M.E. Davis, Facile synthesis and catalysis of pure-silica and heteroatom LTA, Chem. Mater. 27 (2015) 7774–7779, https://doi.org/10.1021/acs.chemmater.5b03579.
[51] J.H. Kwak, R.G. Tonkyn, D.H. Kim, J. Szanyi, C.H. Peden, Excellent activity and selectivity of Cu-SSZ-13 in the selective catalytic reduction of NO_x with NH_3, J. Catal. 275 (2010) 187–190, https://doi.org/10.1016/j.jcat.2010.07.031.
[52] K. Wijayanti, S. Andonova, A. Kumar, J.H. Li, K. Kamasamudram, N.W. Currier, A. Yezerets, L. Olsson, Impact of sulfur oxide on NH_3-SCR over Cu-SAPO-34, Appl. Catal. B-Environ. 166 (2015) 568–579, https://doi.org/10.1016/j.apcatb.2014.11.043.
[53] J.Y. Luo, F. Gao, K. Kamasamudram, N. Currier, C.H.F. Peden, A. Yezerets, New insights into Cu/SSZ-13 SCR catalyst acidity. Part I: Nature of acidic sites probed by NH_3 titration, J. Catal. 348 (2017) 291–299, https://doi.org/10.1016/j.jcat.2017.02.025.
[54] C.H.F Peden, F. Gao, Recent progress in atomic-level understanding of Cu/SSZ-13 selective catalytic reduction catalysts, Catalysts 8 (2018), https://doi.org/10.3390/catal8040140.
[55] F. Gao, N.M. Washton, Y. Wang, M. Kollár, J. Szanyi, C.H.F. Peden, Effects of Si/Al ratio on Cu/SSZ-13 NH_3-SCR catalysts: implications for the active Cu species and the roles of Brønsted acidity, J. Catal. 331 (2015) 25–38, https://doi.org/10.1016/j.jcat.2015.08.004.
[56] T. Zhang, F. Qiu, H. Chang, X. Li, J. Li, Identification of active sites and reaction mechanism on low-temperature SCR activity over Cu-SSZ-13 catalysts prepared by different methods, Catal. Sci. Technol. 6 (2016) 6294–6304, https://doi.org/10.1039/C6CY00737F.
[57] D. Jo, T. Ryu, G.T. Park, P.S. Kim, C.H. Kim, I.S. Nam, S.B. Hong, Synthesis of high-silica LTA and UFI zeolites and NH_3-SCR performance of their copper-exchanged form, ACS Catal. 6 (2016) 2443–2447, https://doi.org/10.1021/acscatal.6b00489.
[58] M.Q. Shen, Y. Zhang, J.Q. Wang, C. Wang, J. Wang, Nature of SO_3 poisoning on Cu/SAPO-34 SCR catalysts, J. Catal. 358 (2018) 277–286, https://doi.org/10.1016/j.jcat.2017.12.008.
[59] Y.L. Shan, X.Y. Shi, Z.D. Yan, J.J. Liu, Y.B. Yu, H. He, Deactivation of Cu-SSZ-13 in the presence of SO_2 during hydrothermal aging, Catal. Today 320 (2019) 84–90, https://doi.org/10.1016/j.cattod.2017.11.006.
[60] T. Ryu, H. Kim, S.B. Hong, Nature of active sites in Cu-LTA NH_3-SCR catalysts: a comparative study with Cu-SSZ-13, Appl. Catal. B-Environ. 245 (2019) 513–521, https://doi.org/10.1016/j.apcatb.2019.01.006.
[61] C. Paolucci, A.A. Parekh, I. Khurana, J.R. Di Iorio, H. Li, J.D. Albarracin Caballero, A.J. Shih, T. Anggara, W.N. Delgass, J.T. Miller, Catalysis in a cage: condition-dependent speciation and dynamics of exchanged Cu cations in SSZ-13 zeolites, J. Am. Chem. Soc. 138 (2016) 6028–6048, https://doi.org/10.1021/jacs.6b02651.
[62] N.H. Ahn, T. Ryu, Y. Kang, H. Kim, J. Shin, I.S. Nam, S.B. Hong, The origin of an unexpected increase in NH_3-SCR activity of aged Cu-LTA catalysts, ACS Catal. 7 (2017) 6781–6785, https://doi.org/10.1021/acscatal.7b02852.
[63] P.S. Hammershoi, A.L. Godiksen, S. Mossin, P.N.R. Vennestrom, A.D. Jensen, T.V.W. Janssens, Site selective adsorption and relocation of SO_x in deactivation of Cu-CHA catalysts for NH_3-SCR, React. Chem. Eng. 4 (2019) 1081–1089, https://doi.org/10.1039/c8re00275d.
[64] Y. Jangjou, C.S. Sampara, Y.T. Gu, D. Wang, A. Kumar, J.H. Li, W.S. Epling, Mechanism-based kinetic modeling of Cu-SSZ-13 sulfation and desulfation for NH_3-SCR applications, React. Chem. Eng. 4 (2019) 1038–1049, https://doi.org/10.1039/c8re00210j.
[65] L. Wei, D.W. Yao, F. Wu, B. Liu, X.H. Hu, X.W. Li, X.L. Wang, Impact of hydrothermal aging on SO_2 poisoning over Cu-SSZ-13 diesel exhaust SCR catalysts, Ind. Eng. Chem. Res. 58 (2019) 3949–3958, https://doi.org/10.1021/acs.iecr.8b04543.
[66] K. Leistner, K. Xie, A. Kumar, K. Kamasamudram, L. Olsson, Ammonia desorption peaks can be assigned to different copper sites in Cu/SSZ-13, Catal. Lett. 147 (2017) 1882–1890, https://doi.org/10.1007/s10562-017-2083-8.
[67] W. Halstead, Thermal decomposition of ammonium sulphate, J. Appl. Chem. 20 (1970) 129–132, https://doi.org/10.1002/jctb.5010200408.
[68] J.E. Schmidt, R. Oord, W. Guo, J.D. Poplawsky, B.M. Weckhuysen, Nanoscale tomography reveals the deactivation of automotive copper-exchanged zeolite catalysts, Nat. Commun. 8 (2017) 1666, https://doi.org/10.1038/s41467-017-01765-0.